Korean J. Chem. Eng., 38(3), 565-575 (2021)
DOI: 10.1007/s11814-020-0721-0

pISSN: 0256-1115
eISSN: 1975-7220

Supported carbon membranes using poly(ether sulfone) precursor

Ana Katiuce Fellenberg*,, Cláudia Leites Luchese**,†, Nilson Romeu Marcilio*, and Isabel Cristina Tessaro****

*Laboratório de Processamento de Resíduos - LPR
**Laboratório de Processos de Separação por Membranas - LASEM
(*Received 4 May 2020 • Revised 19 November 2020 • Accepted 24 November 2020*)

Abstract−This research focused on developing membranes using poly(ether sulfone) as polymeric precursor and DMSO as a solvent. The dip-coating technique was used to form a polymeric layer on the alumina ceramic tube, and the pyrolysis was conducted at 700 °C under N_2 atmosphere. The structural analyses showed that the supported carbon membranes (SCM) are basically composed of amorphous and turbostratic carbon with graphitic domain, confirming the heterogeneity of the matrix. It was observed from the FTIR and XRD results that the precursor polymer was fully pyrolyzed. The carbon structure obtained presented a microporous character (pore radius equal to 6.2 Å) and a high BET surface area (approximately 400 $m^2\ g^{-1}$). The SCM presented a well-defined selective layer with little or no intrusion in the pores of the support. A higher polymeric concentration promoted an increase in the thickness of the carbon membranes (from 20 μm to 36 μm). The carbon membranes produced showed high thermal stability, allowing their application in gas separation processes at higher temperatures, up to approximately 400 °C.

Keywords: Poly(ether sulfone), Dimethylsulfoxide, Pyrolysis, Carbon Membranes, Natural Gas Purification

INTRODUCTION

The increasing energy demand and the growth of the world's population and environmental concerns require new technologies and alternative energy sources with the lowest possible environmental impact. According to the International Energy Agency (IEA), the energy demand will increase by 45% from 2001 to 2030, with an average increase of up to 1.6% per year [1]. In 2009, the overall energy consumption from natural gas (NG) corresponded to 15.6% [2], already in 2013, the percentage of natural gas used in the world energetic matrix was higher, around 24% [3]. The increase in the global demand for NG has required a search for new possibilities. The exploration of unconventional, contaminated, and/or previously considered unviable gas reserves is being re-evaluated in terms of their development potential [4].

NG has already consolidated participation in the world energetic matrix, enabling its use as an alternative for petroleum derivatives (diesel and fuel oil), coal, and nuclear energy [5]. NG is considered clean energy, with lower emission rates, and a significant increase in its offer in world reserves close to oil reserves.

One of the main contaminants in natural gas is carbon dioxide, which should be removed because it can reduce the calorific potential, affecting the operating system and, consequently, the commercialization costs [6]. Also, in the presence of water, the CO_2 becomes acidic and corrosive, being a potentially damaging agent for pipes and equipment. In liquefied natural gas (LNG) processing plants operating at very low temperature, CO_2 can freeze and block the pipelines [7-9]. Different technologies can be used for the purification of natural gas, for instance, amine absorption, adsorption, membrane gas permeation, and cryogenic processes [10, 11]. Compared to other gas separation techniques, membrane gas permeation has several advantages, being considered a cleaner and viable process that allows energy-saving since it does not require phase change to achieve the separation. Furthermore, processes with membrane are more feasible when the natural gas contains high amounts of CO_2 and the gas stream has a moderate flow rate. When the gas flow rate is very high, the amine absorption process is still more viable since the performance parameters of the membranes (permeability and selectivity) are more tightly influenced [12].

Polymeric membranes are generally used for gas permeation due to low cost and high packaging density. However, limitations in separation performance and low stability under more severe operating conditions are the main obstacles for industrial-scale applications. The interest in inorganic membranes arises to overcome these limitations once these membranes have the advantage of being chemically inert and stable at high temperatures [9]. Recently, inorganic carbon membranes have attracted attention due to high selectivity, high hydrophobicity, high-temperature stability, and corrosion resistance [13]. Carbon membranes can be produced in different configurations such as hollow fiber, flat sheet, tubular, supported, or non-supported. Supported carbon membranes consist of a thin selective film deposited on a support, which provides mechanical stability, and they can be prepared by coating ceramic or metallic support with a polymeric solution followed by pyrolysis.

It is important to highlight that pyrolysis operating parameters, such as heating and cooling rate, atmosphere condition, purge gas rate, temperature (intermediary and final) and process time play an important role in the properties of carbon membranes [14]. Pyrolysis temperatures directly influence the structural property, separation performance, and transport mechanism of carbon membranes.

†To whom correspondence should be addressed.
E-mail: claudia.luchese@ufrgs.br

The higher the pyrolysis end temperature, the lower the permeability and the higher the selectivity, since there is a tendency of smaller pore formation. At the same time, high heating rate can lead to the appearance of small holes, cracks, microscopic bubbles, and defects, which in extreme cases can restrict and even preclude the membranes' use [12].

The choice of the polymeric precursor is important since the pyrolysis of different precursors may bring different kinds of carbon membranes. Polymers with a high glass transition temperature (T_g) allow minimizing abrupt changes in the original structure during thermal heating. Moreover, the polymer selected should be able to present graphitization behavior [15-17].

Poly(ether sulfone) (PES) is a vitreous, hydrophilic, and amorphous polymer [18], with high mechanical properties, chemical, and thermal stability [19], besides being commercially available. PES can be considered one of the best known polymeric materials for micro and ultrafiltration and gas separation membranes, since it provides unique properties such as excellent thermal and mechanical resistance, and hydrolytic characteristics in hot-wet environmental [20]. In addition, it presents higher selectivity values for the CO_2/CH_4 gas pair than other polymers, such as polysulfone and cellulose acetate, polymers commonly used in the manufacture of commercial polymeric membranes for gas permeation.

Among the different solvents that can be used for poly(ether sulfone), dimethyl sulfoxide (DMSO) was selected in this work due to its low toxicity when compared to commonly used solvents such as N-methyl pyrrolidone (NMP), dimethylformamide (DMF), dimethylacetamide (DMAc). DMSO is an alternative solvent for the preparation of PES membranes due to its solubility characteristics and good solvent-PES interaction similar to solvents considered more toxic [21].

Several studies have been carried out with PES polymeric membranes; however, to the best of our knowledge, no studies were found in the literature using PES for the development of carbon membranes. Thus, the aim of this work was to study the PES application as a polymeric precursor for the preparation of carbon membranes. The membranes were characterized concerning morphology, chemical structure, thermal property, and also their performance (permeability and selectivity) for single gas permeation tests, focusing on natural gas separation (CO_2/CH_4).

EXPERIMENTAL

1. Materials

PES (Ultrason®E 6020 P) polymer was donated by BASF (Brazil). According to the manufacturer, the molar mass of the PES monomer is 232.26 g mol^{-1} and glass transition temperature (T_g) is 225 °C. Dimethylsulfoxide (DMSO - 99.9% purity - Dynamic) was used as a solvent. DMSO has a high affinity for water and high boiling temperature (T=189 °C to 760 mmHg). Commercial ceramic tubes TCB99 (Tecnicer Cerâmica - Brazil) with 99% (w/w) of alumina (according to manufacturer) sintered at 1,450 °C, with a length of 13.6 cm and external and internal diameters of 1 cm and 0.7 cm, respectively, were used in the preparation of the supported polymeric membranes.

2. Experimental Procedure

The preparation of polymeric solution used as coating of the ceramic tubes involved using different concentrations of PES, 16 and 18% (w/w), and DMSO as a solvent. The polymeric solutions were kept under stirring (30 rpm) using a magnetic stirrer (Fisatom - Brazil) overnight until complete solubilization at ambient temperature.

The polymeric films (PF) were prepared by casting the polymeric solutions in glass Petri dishes, forming a thin layer. The plates were immersed in a non-solvent (distilled water) bath for 3 min. After, the excess of water was removed. The samples were placed in an oven (T=60 °C) for complete evaporation of the solvent and designated as PF16 and PF18 for PES concentration of 16% and 18%, respectively.

The coating of the support using the polymeric solution was performed according to the methodology described in Patent BR 10 2018 009075-5 - Method for forming a dense polymeric layer in porous support. Briefly, the dip-coating process was used to obtain the supported polymeric membranes. Ceramic tubes covered with the polymeric solution (different concentrations) were inserted in a preheated oven (60 °C) with a rotatory shaft (20 rpm). All drying process was conducted using the rotation in order to obtain a more uniform coating, preventing the non-uniform and fast release of solvent, avoiding the formation of bubbles and, consequently, the presence of defects. Also, gravitational effects could be minimized, resulting in membranes with a more homogeneous thickness. The supported polymeric membranes (SPM), SPM16 and SMP18, were submitted to pyrolysis in order to obtain the supported carbon membranes (SCM), SCM16, and SCM18. Similarly, the PFs were pyrolyzed, and the carbon films (CF) were denominated CF16 and CF18, according to the PES concentration solution.

The pyrolysis was conducted in a bipartite vertical tubular furnace (Sanchis, Brazil) until the final temperature of 700 °C under an inert nitrogen atmosphere (N_2 - 99.5%, White Martins) with a flow rate of 2 L min^{-1} measured by a flowmeter device (Omel/P - Brazil). The heating rates used in each pyrolysis step are illustrated in Fig. 1. After reaching room temperature, the SCMs and CFs were removed from the furnace and stored in a desiccator until characterization.

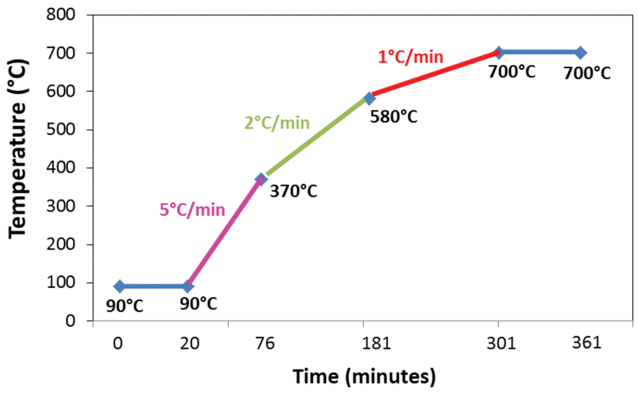

Fig. 1. The protocol of the pyrolysis process: temperature levels and heating rates used for the formation of the supported carbon membranes and carbon films.

3. Physicochemical Characterization

The viscosity of polymeric solutions was analyzed in a SMART rotational viscometer (FUNGILAB S.A.). The readings were recorded for one hour. The viscosity means value corresponds to the average of the viscosity values registered above the data reliability scale (ranging between 70 e 90%) indicated by the manufacturer.

Thermal analysis by differential scanning calorimetry (DSC) was carried out to determine the glass transition temperature (T_g) of the polymeric precursor using the inflection point method. The DSC analysis was performed using a differential scan calorimeter (model DSC 6000, Perkin Elmer) with two heating and cooling slopes and an isothermal plateau between each one. The temperature range was −50 °C to 430 °C. The heating and cooling rates were 10 °C min^{-1}, and the analysis was conducted under an inert nitrogen atmosphere.

To verify the effects of heating on the polymer and the polymeric films, thermogravimetric analysis (TGA) combined with the differential thermal analysis (DTA) (SDT Q600, TA InstrumentsWaters) were performed by submitting the samples to the heating (temperatures between 25 and 800 °C) at a rate of 10 °C min^{-1} under N_2 atmosphere. It was possible to obtain the thermal decomposition temperature (T_d) and the percentage of mass loss.

For chemical structure characterization, Fourier transform infrared spectroscopy (FTIR) of the polymeric films (PF16) and the carbon films (CF16) was performed to verify possible modifications in the chemical structure of the polymer before and after the pyrolysis process. The equipment used was a spectrophotometer (Perkin Elmer-Frontier) in the range of 4,000 to 400 cm^{-1}, 64 scans, and resolution of 4 cm^{-1}. The yield of the CFs in relation to the PFs was calculated by the difference in mass before and after pyrolysis.

The Raman scattering spectroscopy (micro-Raman coupled to an Olympus microscope, laser HeNe − λ=632.8 nm and 10 mW of power) technique was used for analyzing the structural characteristics of the PES polymer and of CF16 and CF18 carbon films. A magnification of 50x and a dot with a diameter of 2-3 μm was used, during 20 s for PES and 30 s for CF. The detection was accomplished by a monochromator (iHR320, Jobin-Yvon) with a charge-coupled device (CCD) detector, refrigerated with liquid nitrogen. In this work, carbon powders obtained by comminution of the carbon films (CF) were used to eliminate the influence of the ceramic support in the results and comply with the requirements necessary to perform the analysis [22].

X-Ray diffraction (D2 Phaser, Bruker) analysis using the power of 30 kV and CuKα radiation with a scan of 0.05° in the region (2θ) ranging from 2° to 90° was performed to assist the characterization of the chemical structure of the CF. For the calculation of the d-spacings, the Bragg law was used, according to Eq. (1):

$$n\lambda = 2d\sin\theta \tag{1}$$

being λ the X-ray wavelength (λ=1.5406 Å for CuKα radiation) and θ the Bragg angle.

Analyses of specific surface area and pore size distribution determined by BET and BJH methodologies were performed for CF16 and CF18 samples. N_2 was used as the adsorbate gas in the Quantachrome (model NOVA 4200e) analyzer. It allows the construction of adsorption and desorption isotherms at 77 K. Prior to the analyses, the samples were heated and degassed under vacuum (approximately 3 h) to promote the complete removal of possible interferents adsorbed on the sample, ensuring accuracy in the measurements.

The morphology of the samples was analyzed by scanning electron microscopy (SEM) using the Leo Evo 50 HV (Carl Zeiss AG) equipment, with a nominal resolution of 3 nm and acceleration tension of 10 kV. From the cross-section morphological analysis and using the dimension scale, it was possible to estimate the thickness of the carbon membranes formed on the support.

4. Performance Tests

The performance of the supported carbon membranes, SCM16 e SCM18, to gas separation was evaluated through pure gas permeation tests: He, N_2, CO_2, and CH_4 (Linde, 99.7%), using a conventional system. The carbon tubular membrane was sealed and placed in a custom-made permeation module. The feed pressure of the gas permeation module was controlled by a pressure regulating valve that allowed a fine adjustment in the range of 0 to 5 bar. The permeation tests were performed in six different samples for each membrane. The permeate flux of the membranes was determined using a timer coupled with a bubble flow meter (indirect measurement) in quadruplicate. For each transmembrane pressure tested, it was assumed that steady-state was reached when time values were constant (a difference less than 5%) and the molar flux of the gas (J_i) in the membrane was calculated using Eq. (2):

$$J_i = \frac{n}{A_m \bar{t}_{ee}} = \frac{pV}{RT}\frac{1}{(\pi D_e L)\bar{t}_{ee}} \tag{2}$$

being p (Pa) and T (K) the room pressure and temperature conditions of the permeate fraction, V (mL) the volume measured in the bubble flow meter, R (atm L mol^{-1} K^{-1}) the universal gas constant, A_m (50.81 m^2) is the external area of the membrane, $\bar{t}_{ee}$ (s) is the average time. The ideal gas equation was used for calculation of the number of moles (n) of gas "i" passing through the membrane.

The molar flux values were plotted as a function of the transmembrane pressure. The angular coefficient represents the permeance, P_i (mol m^{-2} s^{-1} Pa^{-1}), of the gas "*i*" to the membrane, which was converted to GPU. Ideal selectivities (α_{ij}) were obtained by computing the ratio between pure gas permeance, according to Eq. (3):

$$\alpha_{i,j} = \frac{P_j}{P_i} \tag{3}$$

RESULTS AND DISCUSSION

For polymeric solutions prepared using different PES concentrations, 16% and 18%, viscosity values were 1,284 and 2,390 mPa s^{-1}, respectively. The viscosity of a polymeric solution depends on several parameters, such as the average molar mass of the macromolecules, polymer conformation, interactions with the solvent, inter and intramolecular interactions, and concentration of the polymer. The greater the intermolecular forces or the size of the molecules, the greater the internal friction and/or internal kinetic

energy and, therefore, the higher the viscosity [18]. The viscosity of the polymeric solution directly affects the membrane layer formation on the support. It is important to point out that, if the viscosity of the solution is very low, the intrusion of this solution into the support is facilitated, promoting, as a consequence, the formation of an uneven and non-homogeneous layer. However, if the viscosity values of the polymeric solution are too high, the defects can form the structure during the pyrolysis process, such as cracks and/or micro-fissures.

The information about the values of viscosity high and low is nonspecific. Some studies from the literature are presented hereafter to situate the reader in relation to these viscosity values. Lakshmi et al. [19] evaluated the viscosity of a PES (10%, w/w) and DMSO solution used to prepare porous and nanoporous polymeric spheres, and reported the value of 85 mPa s^{-1}. Idris et al. [23] evaluated the viscosity of a solution containing PES (20%, w/w), PEG (as an additive), and DMF as a solvent and found a viscosity of 521 mPa s^{-1}. Ismail et al. [24] evaluated the viscosity of polymeric solutions of P84 (polyimide commercial) and NMP, for the development of supported carbon membranes on discs, in different concentrations of 6, 9, 12, and 15% (w/w), and reported the following viscosity values: 17, 20, 138, and 214 mPa s^{-1}, respectively.

With an increase of only 2% (16 for 18%) in the PES concentration, the viscosity had a substantial increase (almost twice higher). Other authors observed similar behavior comparing the viscosity value of the PES (10%, w/w) solution [19,24]. This abrupt increase in viscosity probably occurred due to the overlapping and interpenetration of molecular chains. Given a certain concentration, this overlap may occur and the rapid transition corresponds to the beginning of the overlap of the spiral between the polymer chains in the solution [25].

In Fig. 2 are displayed the thermal analyses results for pure PES, PF16, and PF18 films. By DSC curves, it was possible to determine the T_g of the samples, and the values obtained were of 227 °C for PES, 225 °C for PF16, and 230 °C for PF18. According to the manufacturer (BASF), the glass transition temperature (T_g) of the PES is 225 °C. Therefore, these results agree with the report by the manufacturer and the literature information [26-30].

As can be seen in TGA curves (temperature ranging between 25 and 800 °C) and the respective derivative curves (DTA) for PES and polymeric films, PF16 and PF18 (Fig. 3), the temperature at the beginning of the degradation for PF samples occurred at values close to 200 °C, with approximately 17% mass loss. Around this temperature, the mass loss can be attributed to the water absorbed and the solvent remaining in the polymeric films [31], since for PES this behavior was not observed. Note that the solvent boiling point (DMSO) is approximately 189 °C.

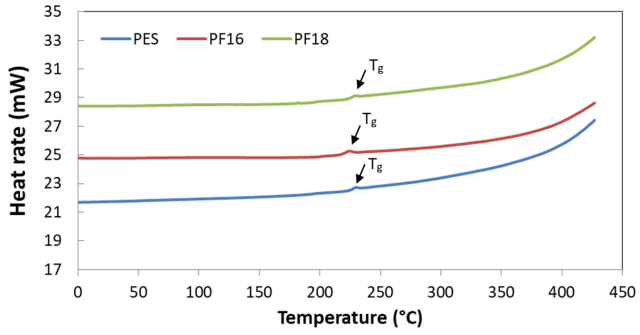

Fig. 2. Differential scanning analysis (DSC) for samples of pure PES, PF16, and PF18 films.

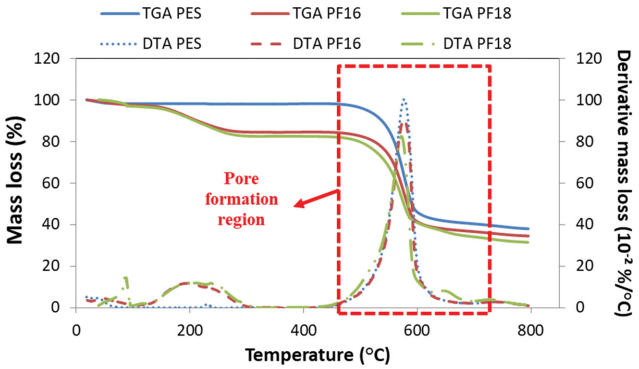

Fig. 3. Thermogravimetric (TGA) and derivative mass loss (DTA) analysis for PES and polymeric films, PF16 and PF18.

The thermal decomposition temperature (T_d) of a polymer is commonly determined using as a criterion the mass loss (5%). In the present work, T_d would be approximately 510°C, evidencing that PES is a polymer resistant to high temperature. The smaller mass losses occurring before T_d are predominantly related to the break of chains of the carbon-sulfur connections between the aromatic rings and the sulfone groups [32].

An expressive loss of mass occurred at a temperature of approximately 450 °C [31,33,34], coincident with the beginning of the pore formation region (as indicated in Fig. 3) due to the rupture of the benzene rings present in the polymer structure. The removal of heteroatoms present in the polymeric structure can promote the release of gas molecules such as CO, CO_2, and CH_4 [32].

The mass loss only begins to reach a plateau when the temperature approaches around 700 °C, generating volatile products such as CO_2, CO, and SO_2 and condensed aromatic residues. At this temperature occurs the stabilization of the mass loss and the residual mass for the PES can be considered 40%. In the last stage, some small fluctuations in mass loss can contribute to the reorganization or rearrangement of graphite sheets in the carbon matrix [32]. Pore creation occurs in the more pronounced mass loss region at a temperature between 450 and 600 °C. Then, a reduction in pore size occurs in the region of the mass loss stabilized at a temperature of about 600 to 700 °C [35]. In addition, approximately 65% of mass loss was observed for the PF samples, regardless of PES concentration. Qadir et al. [34] and Liang et al. [36] found similar mass loss values for polymeric solutions containing PES (15%) in NMP, and PES (20%) in DMF incorporated with TiO_2, respectively.

FTIR analysis was used to investigate changes in the chemical structure of the polymeric precursor when submitted to the pyrolysis process. The spectra of the polymeric film (PF16) and carbon film (CF16) are shown in Fig. 4.

It is possible to observe the characteristic vibration bands of the chemical bonds of the polymeric precursor. The band in the wavenumber region between 3,500-3,700 cm^{-1} can be attributed to the

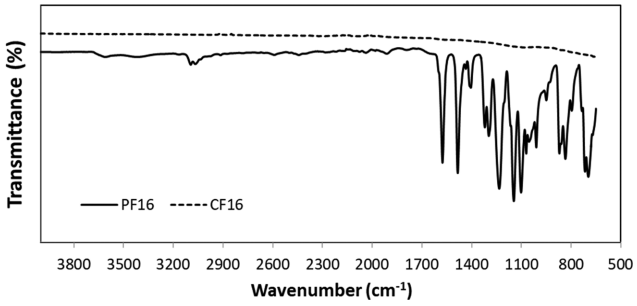

Fig. 4. Fourier Transform Infrared Spectroscopy (FTIR) spectra for polymeric film, PF16, and carbon film, CF16.

O-H stretching [37] related to water molecules remaining in the PF sample, due to the phase inversion process in a distilled water bath, since PES does not have O-H bonds in its structure. Also, porous materials may contain a small amount of water in their pores, almost impossible to remove [38]. The bands observed around 834 and 1,011 cm^{-1} are associated with the C-H deformation of the aromatic ring, and the wavenumbers ranging between 1,484 and 1,576 cm^{-1} are related to stretching C=C [27,32,39]. It is possible to observe bands in the spectral ranges of 2,890-2,918 cm^{-1} and 3,000-3,150 cm^{-1}, referring to C-H stretching [37,40]. The bands at 1,146, 1,297, and 1,320 cm^{-1} are characteristic of the sulfone groups (O=S=O symmetrical and asymmetrical stretching) [39,41], and the band in 1,235 cm^{-1} is associated with the C-O-C stretching of the aromatic ether molecules [39]. The bands at 716 cm^{-1} and 985 cm^{-1} could be attributed to the C-S stretching [42]. From the FTIR spectrum of carbon film, it is possible to verify that all bands practically disappeared. It is possible to confirm that the chemical composition was gradually decomposed from the matrix forming gases such as H_2S, SO_2, CO, and CO_2, among others. The residual structure can be combined and rearranged, leading to the formation of the graphite-like structure. The disordered stacking of this graphite-like structure, such as turbostratic carbon, forming the porous structure of carbon membranes [32]. The characteristic vibrational bands observed in the polymeric membranes decreased and almost disappeared due to the decomposition of the chemicals groups present in the polymeric precursor at high temperatures during the pyrolysis process. This behavior has also been reported by other authors [43-45]. The intensity of the vibrational bands of materials containing carbon is weakened after the carbonization process [22], making difficult the use of FTIR for the characterization of carbon materials structure.

Raman spectroscopy is sensitive to long and short-range crystalline molecular structures. It can be used to characterize the disorder in carbon materials since the ordered and disordered regions of carbonaceous materials present characteristic resonances in the spectrum [46]. Fig. 5(a), (b), and (c) show the Raman spectra for PES and the carbon films, CF16 and CF18, respectively. It is possible to observe in Fig. 5(a) peaks around 1,154 cm^{-1}, referring to the symmetrical stretching of C-O-C and also the peak deformation around 791 cm^{-1}, confirming the molecular structure of PES [47,48]. An extended band in 1,360 cm^{-1} referring to band D (defect) can be observed in Fig. 5(b). At approximately 1,630 cm^{-1}

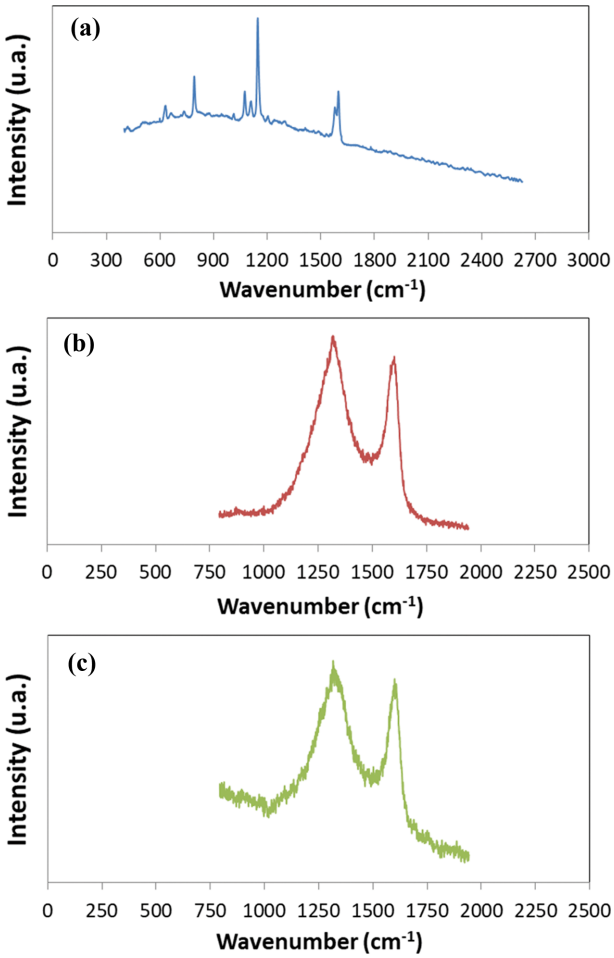

Fig. 5. Raman spectroscopy of (a) PES, and carbon films (b) CF16, and (c) CF18.

it is verified the band G, corresponding to the carbon-graphite structure (carbon with hybridization sp^2) [43]. The presence of D and G bands for CF18 occurred in the identical wavenumbers observed in the spectrum displayed in Fig. 5(c) for CF16.

The D band represents disordered/amorphous structures and the G band represents the graphite structures [22]. The graphite structure presence permits confirming that the carbon membrane was fully carbonized and transformed into a carbon matrix structure [49]. The higher the intensity of D-band, the greater the amount of "disorganized" carbon and the smaller the graphite crystal size. These results indicate that the carbon membranes can be arranged of amorphous carbon [12], carbon graphite [41], vitreous carbon, turbostratic carbon [22], and even graphene oxide [50]. It is important to note that it was not possible to observe the presence of 2D bands, which evidenced the presence of graphene monolayers or a small stacking of blades organized in the carbon membranes. From this result, it is possible to infer that the amount of graphene oxide may be small relative to amorphous carbon [12].

Fig. 6 shows the X-ray diffractograms (XRD) of the carbon films, CF16, and CF18. The behavior of the curves is characteristic of turbostratic structures, with amorphous and microcrystalline carbon domains. The hexagonal planes are not aligned but rather

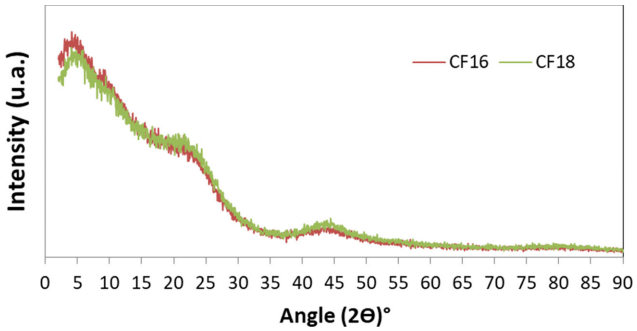

Fig. 6. X-ray diffractogram of carbon films, CF16 and CF18.

shifted from each other or overlapping, conferring a highly disordered character to the material [45].

It can be observed that the diffractograms of carbon films presented two widened bands, typical of amorphous material [51,52]. This result indicates that X-rays are scattered in several directions, promoting effective collisions distributed in a wide range (2θ), rather than the formation of narrower peaks with high intensity. The wide diffraction peak at 2θ=15-30° can be attributed to amorphous carbon structures [53]. The wide and weak diffraction peak at 2θ=40-50° occurs due to the *a*-axis of the graphite structure [54]. In the XRD standards, the position of the diffraction peak (002) in the plane is around $2\theta\approx21.6°$ for the CF16 and $2\theta\approx20.7°$ for the CF18. According to the Bragg Equation, the calculated value of interlayer distance d002 is 0.411 nm for CF16 and 0.429 nm for CF18, much higher than pure graphite (0.354 nm) [53]. This result indicates the low degree of graphitization of the carbon material formed [55].

The widened peak at $2\theta\approx44°$ with weak intensity, characteristic of graphite plane (100), suggests that a three-dimensional ordered rudimentary structure was formed. This also implies that a graphite-like structure was formed in the turbostratic carbon matrix. The more intense and noticeable $2\theta\approx44°$ peaks, the more graphitization occurred, indicating that the polymeric precursor used is a graphitized carbonaceous material [24,53,56]. This band at $2\theta\approx44°$ represents the carbon-carbon spacing of the graphite planes, indicating that the material has aromatic compounds in the planes with a more ordered and better-conditioned structure [45]. Also, this peak determines the carbon-carbon spacing of the planes, being possible to determine the longitudinal measurement of the structural elements. In this case, for CF16 and CF18 samples, the d space in the plane (100) has values of 0.208 and 0.209 nm, respectively; for graphite, this value is 0.204 nm [45].

To characterize the carbonaceous material, in Fig. 7(a) and (b) are displayed the adsorption and desorption isotherms of N_2 at 77 K for the carbon films, CF16 and CF18, respectively. Isotherms can be classified into six main categories according to the IUPAC classification scheme. Fig. 7 represents a type of physical adsorption corresponding to the isotherm type I which is related to microporous materials [57]. Type I isotherm is concave to the axis of relative pressure (P/P_o), and the absorbed amount has the tendency to approach a limit value. In Fig. 8(a) and (b) are displayed the pore size distributions for the CF16 and CF18 samples, respectively, determined from sorption results.

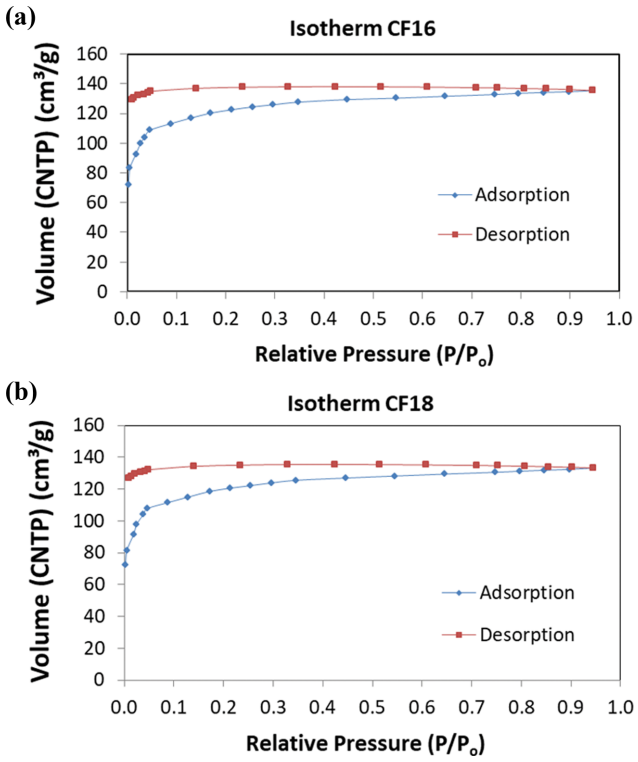

Fig. 7. N_2 adsorption and desorption isotherms for the carbon films (a) CF16 and (b) CF18.

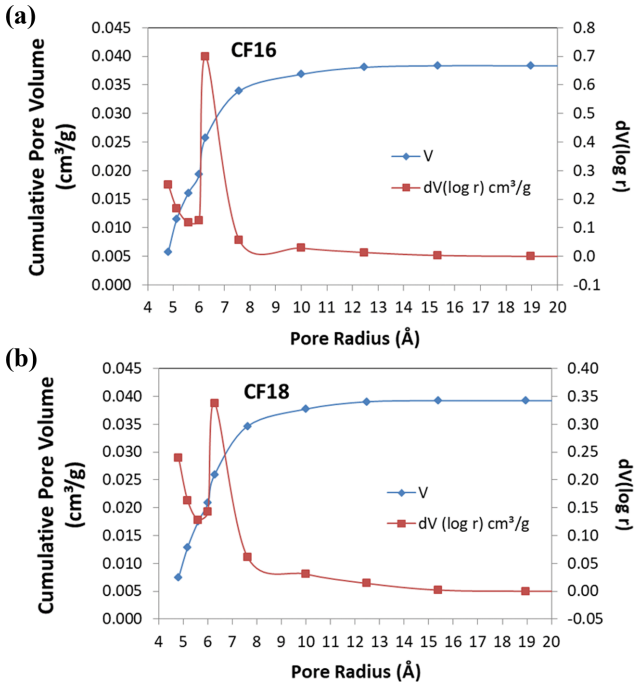

Fig. 8. Pore size distribution of carbon films (a) CF16 and (b) CF18.

A narrow and centralized pore size distribution was observed in the carbon films, regardless of polymeric solution concentration. Table 1 shows the pore size and specific surface area values for the

Table 1. BET parameters for the pore structure of carbon films CF16 e CF18

Sample	Surface area BET (m^2/g)	Total pore volume (cm^3/gs)	Pore radius (Å)	Pore size diameter (nm)
CF16	401.03	0.038	6.25	1.2508
CF18	393.9	0.039	6.27	1.2542

carbon films CF16 and CF18.

It is well known that the pores can be classified according to the diameter, being named micropore samples with pore diameter smaller than 2 nm. Mesopores have a diameter ranging between 2 and 50 nm, and macropores have a diameter higher than 50 nm. From the data of Table 1 and the results in Fig. 8, it is possible to suggest that the carbon films CF16 and CF18 have porous structures formed by micropores with a high surface area. The photographs (visual aspect) of the ceramic tube TCB99, supported polymeric membranes (SPM16 and SPM18), and supported carbon membranes (SCM16, and SCM18), and their respective surface morphologies are depicted in Fig. 9.

It is possible to observe in TCB99, Fig. 9(a), a porous surface composed of irregularities. Comparing the micrographs of the ceramic tube and the supported polymeric membranes, SPM16 and SPM18, in Fig. 9(a), (b), and (c), an apparently smoother surface is observed, suggesting that the coating is satisfactory. In Fig. 9(c), for SCM16 and SCM18 samples, it is possible to observe a uniform external surface with some fractures and cracks.

Moreover, it is possible to observe an increase in the size of the fracture for SCM18, probably related to the thickness of the carbon membrane, which is influenced by different factors such as the viscosity of polymeric solution [58], pyrolysis conditions, and the nature of the polymeric precursor [46,59]. This effect can also be explained by the low yield of the carbon films, 34% for CM16, and 33% for CM18. These observations are in accordance with the thermogravimetric results for the polymeric precursor. Thus, the loss of mass in the pyrolysis step is very high (about 60%), promoting fractures in the structure of the supported carbon membrane.

The cross-sections of the carbon membranes, SCM16 and SCM18, are shown in Fig. 10. The complete adherence of the carbon layer in the ceramic support was observed. This is a required condition for membrane use [46,60]. Moreover, it is possible to verify an expressive increase in the selective layer (red arrows) thickness of SCM18. The thickness of the SCM16 membrane was

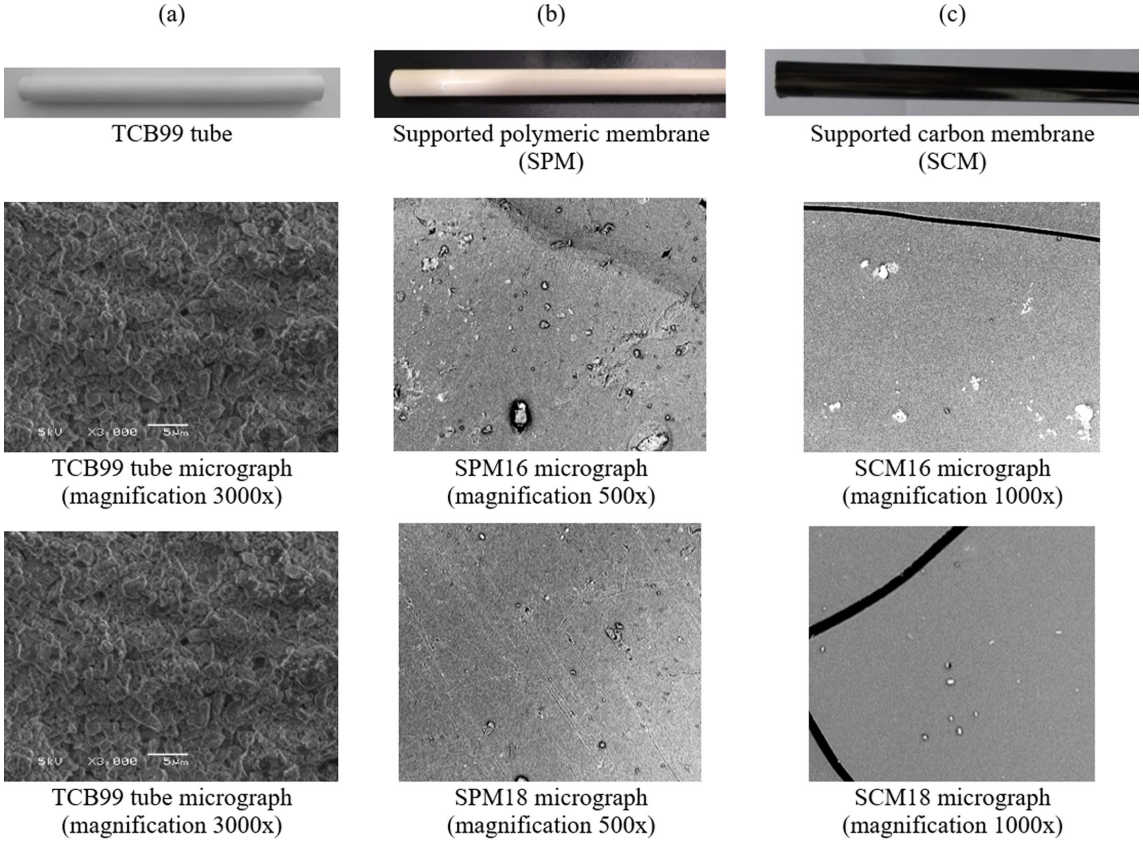

Fig. 9. Photographs and micrographs of the external surface (a) of the ceramic tube TCB99 (3000x) [46], (b) external surface of the supported polymeric membranes, SPM16 (500x) and SPM18 (500x), (c) surface of the supported carbon membrane SCM16 (1000x) and SCM18 (1000x).

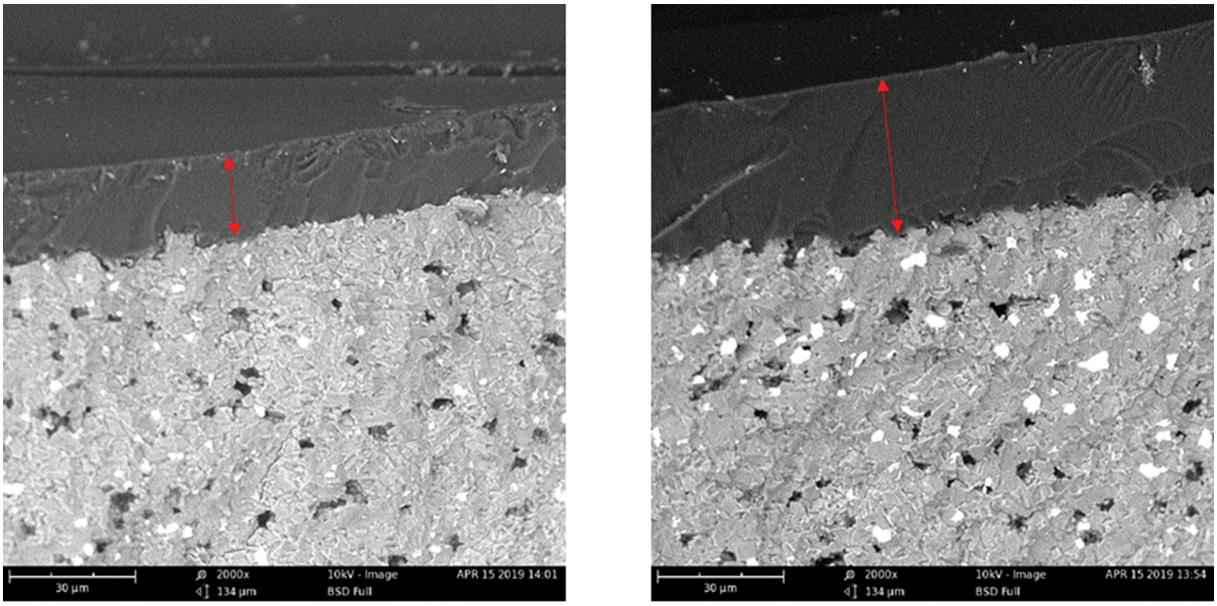

(a) (b)

Fig. 10. Cross-section micrographs of the supported carbon membranes (a) SCM16 and (b) SCM18 (magnification of 2000x).

~20 µm, whereas, for SCM18, the thickness was ~36 µm. Similar thickness (21.3 µm and 35 µm, respectively) values were obtained by other authors using poly(furfuryl alcohol) [61] and phenolic resin [62]. However, the thickness obtained can be considered high compared to those generally reported in the literature. The thickness of the carbon membrane obtained by Hamm et al. [12] from poly(ether imide), pyrolyzed at 800 °C, was approximately 5 µm and at 600 °C, was 22 µm. Ismail et al. [49] reported carbon membrane thicknesses (supported in discs) of 3.2, 5.6, 8.3, and 16.9 µm, using different concentrations (6, 9, 12, and 15%, respectively) of polymeric solutions (P84 and NMP); the authors attributed the increase in carbon membrane thickness to the increase in viscosity. So, it was observed that the higher the viscosity of the polymeric solution, the greater the thickness of the carbon membrane.

In Table 2 are presented the permeance results and the ideal selectivity for SCM16 and SCM18 membranes after permeation tests with different gases (He, N_2, CO_2, and CH_4). For the SCM16 and SCM18 membranes, the highest permeance was for CO_2, followed by CH_4, N_2, and He. According to Centero and Fuentes [63], the high permeation rate was for He, followed by CO_2 and CH_4, different from this work. The higher permeance of CO_2 gas compared to CH_4, N_2, and He gases occurs since CO_2 has greater condensability than the gases CH_4, N_2, and He, reflected by their critical temperatures of approximately 304, 191, 156 and 5 K, respectively [46]. Gases with higher critical temperatures tend to have a more pronounced sorption and permeate more quickly through the membrane [13]. In carbon membranes, gas sorption will depend on the condensability of the penetrating gas (critical temperature), its interactions with the membrane, and the structure of the pores. This effect is predominant when the mechanism of the carbon membranes separation is selective adsorption or surface diffusion ($Ø_P$<2 nm) [12]. Lee et al. [64] prepared carbon membranes of Novalac phenolic resin by pyrolysis at 700 °C, and the permeation rate decreased as follows: He, CO_2, N_2, O_2, CH_4, and SF_6. For CO_2, N_2, and O_2, the permeance was very similar to about 300 GPU. Ismail et al. [24] obtained CO_2 permeance of 400 GPU for a supported carbon membrane obtained by pyrolysis of the P84 polymeric precursor at 700 °C.

Regarding the concentration of the polymeric precursor (PES), there was a decrease in gas permeance as the concentration of PES increased, except for CH_4 that permeation rate remained constant. This behavior differs from that reported by Hamm et al. [46] using a similar pyrolysis condition; there was an increase in gas permeance through the carbon membranes as the concentration of PEI in the polymeric solution increased.

The ideal selectivity to CO_2/CH_4 was similar for SCM16 (1.56) and SCM18 (1.36) membranes. A similar CO_2/CH_4 ideal selectivity was reported by Lee et al. [64], for a carbon membrane obtained at 700 °C using Novalac phenolic resin and a disc of alumina as support. Wey et al. [65] also obtained selectivity values

Table 2. Permeance values and ideal selectivities for supported carbon membranes SCM16 and SCM18

Samples	Permeance (GPU)				Ideal Selectivity			
	He	N_2	CO_2	CH_4	He/N_2	CO_2/N_2	N_2/CH_4	CO_2/CH_4
SCM16	50.8	56.7	116.5	74.7	0.89	2.05	0.76	1.56
SCM18	44.8	50.8	101.5	74.7	0.88	2.00	0.68	1.36

similar to those found in this work for the CO_2/CH_4 gas pair; the carbon membranes were obtained using PEI (10%, w/w), alumina disks (sintered at 1,500 °C) as support and a pyrolysis temperature of 600 °C resulting in the selectivity of 1.8. The highest CO_2/CH_4 selectivity found for these authors was 56 when the alumina support was sintered at 1,400 °C, using the different heating rates in the sintering step. Zainal et al. [56] obtained carbon membranes using a blend of PEI and PEG in different proportions (PEG : PEI ratios of 0, 10, 20, and 30%), with alumina disks as support. The obtained membranes presented ideal selectivity for the CO_2/CH_4 gas pair of 2.4, 4.9, 4.4, and 0.7, respectively. Liu et al. [54] tested the performance of carbon membranes from different polymeric precursors for gas separation; the ideal selectivity value for He/N_2, N_2/CO_2, and CH_4/CO_2 varied from 1.9 to 9.2, 1.3 to 2.4, and 1.5 to 4.8, respectively. Hamm et al. [46] produced supported carbon membranes using PEI under different pyrolysis conditions; the ideal selectivity at 600 °C was 1.7 to 3.4 for He/N_2, 1.5 to 1.9 for He/CO_2, 0.9 to 2.2 for CO_2/N_2, and 0.6 to 1.2 for the pair of CO_2/CH_4 gases. The values obtained for the carbon membranes pyrolyzed at 800 °C were 1.9 to 2.4 for He/N_2, 2.2 to 2.5 for He/CO_2, 0.9 to 1.1 for CO_2/N_2, and 0.6 to 0.7 for CO_2/CH_4.

The ideal selectivity values for all gases were relatively low compared to the values found in the literature. Kiyono et al. [66] reported ideal selectivity values for CO_2/CH_4 ranging between 55 and 75, for CMSM prepared by pyrolysis, in three different atmospheres (He, air, and vacuum), using 6FDA/BPDA-DAM as a polymeric precursor. Ismail et al. [49] obtained selectivity values for CO_2/N_2 and CO_2/CH_4 of 15 and 45, respectively, for a flat supported carbon membrane using P84 as a polymeric precursor. Hosseini et al. [67] evaluated the performance of gas separation for carbon membranes produced from combinations of PBI and other three commercial polymers: Kapton (DuPont), UIP-R (Ube Industries Ltd.), and P84 HT (HP Polymer GmbH); the selectivity for the pairs N_2/CH_4, CO_2/CH_4, CO_2/N_2 ranged from 1.5 to 3.1, 13 to 75, and 8 to 24, respectively.

Molecular sieve, selective adsorption or surface diffusion, and Knudsen diffusion are the most widely accepted transport mechanisms for carbon membranes. These mechanisms can coexist depending on the chemical structure of the material and the properties of the gases evaluated. The ideal selectivity results indicate that the SCM did not have a molecular sieve behavior because the separation factors were relatively low. Molecular sieve transport occurs when the average pore size is smaller than 6 Å. In the selective adsorption mechanism, the gas adsorbs on the internal pore surface, and then, the diffusion occurs through the membrane. The Knudsen diffusion is favored when the average pore size is lower than 50 nm, and in this case, the separation factor can be related to the molar mass of the gases [12].

Comparing the ideal selectivity values and the kinetic diameters of the gases (He=2.6 Å; CO_2=3.30 Å; N_2=3.64 Å and CH_4= 3.80 Å), it was possible to observe that the adsorption has a greater influence than the kinetic diameter, evidencing the predominant transport by selective adsorption, since CO_2 presented greater permeability for both CMs. The critical relative temperature of CO_2 is higher than the other gases tested, promoting a quicker absorption and transport of this gas by the carbon membrane compared to others. Analyzing the selectivity results, it is clear that the values were close to some but lower than several of the selectivity values reported in the literature. It is possible to relate this result with the presence of defects.

The permeation test results show that the samples did not present the molecular sieve mechanism as desired for a carbon membrane. However, it is important to highlight that the SCMs have a relatively larger permeation area than most membranes reported in the literature [24,56,65,68,69]. This greater permeation area can hinder the defect control, making it difficult to obtain a completely homogeneous structure during the coating and pyrolysis steps. Also, other factors can limit the production of an effective membrane, for instance, equipment limitation (fine-tuning for temperature control and gas flowrate control), lack of reproducibility once the process is not mechanized, different properties of the commercial support and other materials used in the manufacture of the membranes [46].

CONCLUSIONS

The results obtained in the present work indicate that the supported carbon membranes were stable at the pyrolysis temperatures used, and the support used did not offer resistance to gas transport. The chosen polymeric precursor, PES, presented a low performance of forming the carbon membrane, once the yield in the carbon matrix was low. Moreover, there was the appearance of cracks in the surface of the supported carbon membrane, probably related to the solution viscosity, pyrolysis conditions, and/or the intrinsic characteristics of PES. The selective layer of the membranes well adhered to the support and with small or no intrusion into the ceramic support. The modification of the chemical structure of PES after the pyrolysis process was verified by the FTIR technique. The formation of a carbon structure apparently without residuals of the polymeric precursor occurred, indicating that the pyrolysis process effectively transformed the polymeric matrix into a carbon matrix. This result was confirmed by XRD analysis. The analysis of the morphology and structure of the formed carbon material showed that the carbon films are basically composed of amorphous and turbostratic carbon, with graphitic domains, confirming the heterogeneity of the carbon matrix. The carbon structure after pyrolysis has a high surface area. Moreover, it was possible to ascertain by the BJH method that the pore structure is formed by micropores, with an average pore diameter around 1.2 nm. The carbon films produced showed high thermal stability, allowing the application of these membranes in gas separation processes at higher temperatures, up to approximately 400 °C. Performance permeation tests using pure gases (He, CO_2, N_2, and CH_4) indicated the formation of a porous structure in the SCM, being the selective adsorption probably the predominant permeation mechanism. The ideal selectivity results obtained for all gas pairs tested did not present satisfactory performance to act as molecular sieves for all membranes. Factors such as the membrane area and the difficulties encountered in the membranes' manufacturing processes imply the generation of defects. In gas separation processes, these limitations can be determinant for membrane performance. The results demonstrate that the technique

proposed and used to develop the carbon membranes has a high potential in gas separation processes. However, it is necessary to improve the selectivity parameters of the membranes developed by using additives or even a polymer blend, to improve the characteristics of the polymeric precursor, to the parameters of the pyrolysis process, to optimize the process and the final membrane properties. Further studies should be carried out to broaden the research on the different polymeric precursors that can be used, as well as possible combinations, looking for improving the performance of the developed carbon membranes and the improvement of the manufacturing techniques.

ACKNOWLEDGEMENTS

The authors acknowledge the Conselho Nacional de Desenvolvimento Científico e Tecnológico (CNPq), the Coordenação de Aperfeiçoamento de Pessoal de Nível Superior (CAPES), and the Fundação de Amparo à Pesquisa do Estado do Rio Grande do Sul (FAPERGS) of Brazil.

DECLARATION OF INTEREST

The authors declare that there are no scientific or financial conflicts of interest.

NOMENCLATURE

$\bar{t}_{ee}$: average of four times measured in stationary state [s]
α_{Kd} : Knudsen separation factor
A_m : external membrane área [m²]
D_e : external diameter of ceramic tube [cm]
J_i : molar flux of component *i* [mol s m^{-2}]
P/P_0 : relative pressure
P_i : gas permeance of compound *i* in the membrane [mol m² s Pa]
P_j : gas permeance of compound *j* in the membrane [mol m² s Pa]
α_{ij} : Ideal selectivity between two pure gases (*i* and *j*)
bcf/d : billion cubic feet/day
GPU : gas permeation unit [GPU=10^{-6} cm^3 (STP) cm^{-2} s^{-1} $cmHg^{-1}$]
ppmv : parts per million by volume
scf/d : standard cubic feet/day
λ : X-ray wavelength [cm^{-1}]
L : ceramic tube length [cm]
R : universal gas constant [atm L mol^{-1} K^{-1}]
d : layer d spacing [Å]
n : moles of gas *i* that pass through the membrane [mols]
θ : bragg angle [°]

REFERENCES

1. M. A. A. Hamid, Y. T. Chung, R. Rohani and M. U. M. Junaidi, *Sep. Purif. Technol.*, **209**, 598 (2019).
2. W. C. Francisco, *Gás Natural, Bras. Esc.*, Fundação Getulio Vargas (2019).
3. S. C. Pessoa, *Gás Natural, Mundo Educ.*, Fundação Getulio Vargas (2019).
4. T. E. Rufford, S. Smart, G. C. Y. Watson, B. F. Graham, J. Boxall, J. C. D. Costa and E. F. May, *J. Pet. Sci. Eng.*, **94**, 123 (2012).
5. R. A. Amaral, A. C. Habert and C. P. Borges, *Chem. Eng. Process. Process Intensif.*, **102**, 202 (2016).
6. M. Wang, Z. Wang, S. Zhao, J. Wang and S. Wang, *Chin. J. Chem. Eng.*, **25**, 1581 (2017).
7. Y. Alcheikhhamdon and M. Hoorfar, *Chem. Eng. Process. Process Intensif.*, **120**, 105 (2017).
8. J. Haider, S. Saeed, M. A. Qyyum, B. Kazmi, R. Ahmad, A. Muhammad and M. Lee, *Renew. Sustain. Energy Rev.*, **123**, 109771 (2020).
9. B. Shimekit and H. Mukhtar, *Natural gas purification technologies - major advances for CO_2 separation and future directions*, H. Al-Megren Ed., In Tech (2012).
10. M. Arjmandi, M. Pakizeh and O. Pirouzram, *Korean J. Chem. Eng.*, **32**, 1178 (2015).
11. S. Mosleh, G. Khanbabaei, M. Mozdianfard and M. Hemmati, *Iran. Polym. J.*, **25**, 977 (2016).
12. J. B. S. Hamm, A. Ambrosi, J. G. Griebeler, N. R. Marcilio, I. C. Tessaro and L. D. Pollo, *Int. J. Hydrogen Energy*, **42**, 24830 (2017).
13. A. F. Ismail and L. I. B. David, *J. Memb. Sci.*, **193**, 1 (2001).
14. W. Zhou, M. Yoshino, H. Kita and K. Okamoto, *J. Memb. Sci.*, **217**, 55 (2003).
15. Y. Yang, T. H. Le, F. Kang and M. Inagaki, *Carbon*, **111**, 546 (2017).
16. D. Hulicova and A. Oya, *Carbon*, **41**, 1443 (2003).
17. T. H. Le and H. Yoon, *Carbon*, **152**, 796 (2019).
18. G. Arthanareeswaran and V. M. Starov, *Desalination*, **267**, 57 (2011).
19. D. S. Lakshmi, A. Figoli, M. G. Buonomenna, G. Golemme and E. Drioli, *Adv. Polym. Technol.*, **31**, 231 (2012).
20. N. A. Alenazi, M. A. Hussein, K. A. Alamry and A. M. Asiri, *Des. Monomers Polym.*, **20**, 532 (2017).
21. N. Evenepoel, S. Wen, M. T. Tsehaye and B. V. D. Bruggen, *J. Appl. Polym. Sci.*, **2**, 1 (2018).
22. W. Jiao, Y. Ban, Z. Shi, X. Jiang, Y. Li and W. Yang, *J. Membr. Sci.*, **533**, 1 (2017).
23. A. Idris, N. M. Zain and M. Y. Noordin, *Desalination*, **207**, 324 (2007).
24. N. H. Ismail, W. N. W. W. Salleh, N. Sazali and A. F. Ismail, *J. Ind. Eng. Chem.*, **57**, 313 (2018).
25. A. S. Sultan, A. Al-Ahmed and S. M. J. Zaidi, *Eur. Polym. J.*, **47**, 2295 (2011).
26. A. L. Ahmad, A. A. Abdulkarim, B. S. Ooi and S. Ismail, *Chem. Eng. J.*, **223**, 246 (2013).
27. A. F. Ismail, R. A. Rahim and W. A. W. A. Rahman, *Sep. Purif. Technol.*, **63**, 200 (2008).
28. H. A. Mannan, H. Mukhtar and T. Murugesan, *Appl. Mech. Mater.*, **625**, 172 (2014).
29. S. Mazinani, R. Ramezani, S. Darvishmanesh, G. F. Molelekwa, R. D. Felice and B. V. D. Bruggen, *J. CO_2 Util.*, **27**, 536 (2018).
30. H. Zangeneh, A. A. Zinatizadeh, S. Zinadini, M. Feyzi and D. W. Bahnemann, *React. Funct. Polym.*, **127**, 139 (2018).
31. M. Liu, Z. Wang, J. Mei, J. Xu, L. Xu, H. Han, H. Ni and S. Wang, *J. Membr. Sci.*, **505**, 138 (2016).
32. B. Zhang, G. Shen, Y. Wu, T. Wang, J. Qiu, T. Xu and C. Fu, *Ind. Eng. Chem. Res.*, **48**, 2886 (2009).
33. S. Velu, L. Muruganandam and G. Arthanareeswaran, *Brazilian J.*

Chem. Eng., **32**, 179 (2015).
34. D. Qadir, H. Mukhtar and L. K. Keong, *Procedia Eng.*, **148**, 588 (2016).
35. M. A. Ahmad, N. Khalilah, A. Rashid, W. Hafiz, F. Wan, B. H. Hameed and E. Campus, *Int. J. Basic Appl. Sci.*, **10**, 4 (2010).
36. C. Liang, P. Uchytil, R. Petrychkovych, Y. Lai, K. Friess, M. Sipek, M. M. Reddy and S. Suen, *Sep. Purif. Technol.*, **92**, 57 (2012).
37. M. A. Mohamed, W. N. W. Salleh, J. Jaafar, S. E. A. M. Asri and A. F. Ismail, *RSC Adv.*, **5**, 29842 (2015).
38. A. Rahimpour and S. S. Madaeni, *J. Membr. Sci.*, **360**, 371 (2010).
39. S. Hasanajili, M. Latifzadeh and M. Bahmani, *Chin. J. Chem. Eng.*, **25**, 1750 (2017).
40. N. Sazali, W. N. W. Salleh, A. F. Ismail, N. H. Ismail, M. A. Mohamed, N. A. H. M. Nordin, M. N. M. Sokri, Y. Iamoto, and S. Honda, *Chem. Eng. Res. Des.*, **140**, 221 (2018).
41. H. Bai, H. Wang, J. Zhang, C. Wu, J. Zhang, Y. Xiang and S. Lu, *J. Membr. Sci.*, **558**, 26 (2018).
42. R. K. Singh, K. Kunimatsu, K. Miyatake and T. Tsuneda, *Macromolecules*, **49**, 6621 (2016).
43. J. S. Adams, A. K. Itta, C. Zhang, G. B. Wenz, O. Sanyal and W. J. Koros, *Carbon*, **141**, 238 (2019).
44. W. Qiu, K. Zhang, F. S. Li, K. Zhang and W. J. Koros, *ChemSusChems.*, **7**, 1186 (2014).
45. P. S. Rao, M.-Y. Wey, H.-H. Tseng, I. A. Kumar and T.-H. Weng, *Micropor. Mesopor. Mater.*, **113**, 499 (2008).
46. J. B. S. Hamm, A. R. Muniz, L. D. Pollo, N. R. Marcilio and I. C. Tessaro, *Carbon*, **119**, 21 (2017).
47. Y. Manawi, V. Kochkodan, E. Mahmoudi, D. J. Johnson, A. W. Mohammad and M. A. Atieh, *Sci. Rep.*, **7**, 1 (2017).
48. D. S. Lakshmi, T. Cundari, E. Furia, A. Tagarelli, G. Fiorani, M. Carraro and A. Figoli, *Macromol. Symp.*, **357**, 159 (2015).
49. N. H. Ismail, W. N. W. Salleh, N. Sazali, A. F. Ismail, N. Yusof and F. Aziz, *Sep. Purif. Technol.*, **195**, 295 (2018).
50. J. Wu, M. Lin, X. Cong, H. Liu, P. Tan and M. Lin, *R. Soc. Chem.*, **47**, 1822 (2018).
51. A. S. Rajan, S. Sampath and A. K. Shukla, *Energy Environ. Sci.*, **7**, 1110 (2014).
52. M. A. L. Tanco, D. A. P. Tanaka, S. C. Rodrigues, M. Texeira and A. Mendes, *Int. J. Hydrogen Energy*, **40**, 5653 (2015).
53. B. Zhang, Y. Wu, Y. Lu, T. Wang, X. Jian and J. Qiu, *J. Membr. Sci.*, **474**, 114 (2015).
54. X. Y. Liu, M. Huang, H. L. Ma, Z. Q. Zhang, J. M. Gao, Y. L. Zhu, X. J. Han and X. Y. Guo, *Molecules*, **15**, 7188 (2010).
55. B. Zhang, Y. Shi, Y. Wu, T. Wang and J. Qiu, *J. Appl. Polym. Sci.*, **131**, 39925 (2014).
56. W. N. H. W. Zainal, S. H. Tan and M. A. Ahmad, *Chem. Eng. Technol.*, **40**, 94 (2017).
57. F. Mohammadnezhad, M. Feyzi and S. Zinadini, *J. Ind. Eng. Chem.*, **71**, 99 (2019).
58. L. Li, C. Song, H. Jiang, J. Qiu and T. Wang, *J. Membr. Sci.*, **450**, 469 (2014).
59. F. Aziz and A. F. Ismail, *Mater. Sci. Semicond. Process.*, **39**, 416 (2015).
60. C. Wang, X. Hu, J. Yu, L. Wei and Y. Huang, *Ceram. Int.*, **40**, 10367 (2014).
61. M. B. Shiflett and H. C. Foley, *Science*, **285**, 1902 (1999).
62. W. Wei, G. Qin, H. Hu, L. You and G. Chen, *J. Membr. Sci.*, **303**, 80 (2007).
63. T. A. Centeno and A. B. Fuertes, *Carbon*, **38**, 1067 (2000).
64. P. Lee, D. Kim, S. Nam and R. R. Bhave, *Micropor. Mesopor. Mater.*, **224**, 332 (2016).
65. M.-Y. Wey, H.-H. Tseng and C. Chiang, *J. Membr. Sci.*, **453**, 603 (2014).
66. M. Kiyono, P. J. Williams and W. J. Koros, *J. Membr. Sci.*, **359**, 2 (2010).
67. S. E. Hosseini and M. A. Wahid, *Energy Convers. Manage.*, **74**, 426 (2013).
68. Y. J. Fu, C. C. Hu, D. W. Lin, H. A. Tsai, S. H. Huang, W. S. Hung, K. R. Lee and J. Y. Lai, *Carbon*, **113**, 10 (2017).
69. N. Ismail, W. Salleh, N. Sazali and A. F. Ismail, *Chem. Eng. Trans.*, **45**, 1465 (2015).